2024 14th Workshop on Hyperspectral Imaging and Signal Processing: Evolution in Remote Sensing (WHISPERS) | 979-8-3315-1313-9/24/$31.00 ©2024 IEEE | DOI: 10.1109/WHISPERS65427.2024.10876530

IMPROVING SPECTRAL UNMIXING PERFORMANCE BY FREQUENCY COMPONENT REDUCTION

Zakaria Bnoulkacem[1] Bikram Koirala[1], Paul Scheunders[1]

[1] Imec-Visionlab, University of Antwerp (CDE) Universiteitsplein 1, B-2610 Antwerp

ABSTRACT

This paper introduces a novel preprocessing method to reduce the redundancy of spectral data with the purpose of improving the accuracy of hyperspectral unmixing techniques. The approach is based on Fast Fourier Transform (FFT) component selection using a genetic algorithm. The method is tested on a real-world hyperspectral dataset, showing significant reductions in error for multiple unmixing models. Additionally, the method's robustness to noise is evaluated, demonstrating stability under moderate noise levels.

Index Terms— Hyperspectral, unmixing, intimate mixtures, Fast Fourier Transform, genetic algorithms

1. INTRODUCTION

Spectral unmixing is extensively used as a hyperspectral image analysis tool for the quantification of the composition of mixed pixels. The most commonly used unmixing algorithm is the linear mixing model. Under the assumption that each ray of light interacts once with the material before reaching the sensor, the linear model describes a spectrum as a linear mixture of pure endmember specta and their respective abundances. Most commonly, the non-negativity and sum to one physical constraints are added to the model, thus creating the Fully Constrained Least-Squares Linear Unmixing (FCLSLU) model [1, 2] .

To tackle the complexity of more realistic scenarios of multiple light-material interactions, unmixing models like bilinear models [3, 4] (e.g., Polynomial Post-Nonlinear model (PPNM) [5]), and the multi-linear model (MLM) [6] were proposed. The bilinear model assumes that an incident ray of light interacts with two pure materials each time, while the multi-linear model takes into consideration higher-order interactions. In addition to these unmixing models, physical models dealing with intimate mixtures have also been developed, such as the Hapke model [7, 8].

In addition, to deal with the non-linearity of the data, some supervised techniques that rely on neural networks [9, 10, 11, 12] have been developed. Data-driven approaches offer a solid alternative to the physical models discussed before, making use of the flexibility of machine learning techniques to capture the complex interactions between light and the mixed materials.

In the search for better results, preprocessing techniques have been proposed to boost the performance of spectral unmixing. In [13], it was demonstrated that applying a denoising step before unmixing yields lower errors. Other researchers [14] proposed a spatial preprocessing step to improve the unmixing of remote sensing data.

A major problem of hyperspectral data is the high spectral redundancy and the correlation between spectra, caused e.g. by environmental and acquisition conditions, affecting all spectra uniformly. In this work, we aim to reduce these effects with the purpose of improving the task of spectral unmixing. For this, we propose a preprocessing approach based on Fast Fourier transform (FFT) component selection using a genetic algorithm. To remove redundant frequency components, a fitness function that favours orthogonality of the data is proposed. We demonstrate that this procedure reduces the correlation of the data and improves the unmixing.

2. FFT COMPONENT SELECTION USING GENETIC ALGORITHM

2.1. Background

Suppose we have a hyperspectral dataset $\mathbf{Y}$ of N samples $\{\mathbf{y}_i\}_{i=1}^{N} \in \mathbf{R}_{+}^{d}$) of d spectral bands. The data can be modeled as:

$$\mathbf{Y} = F(\mathbf{E}, \mathbf{A}) + \mathbf{e}, \tag{1}$$

where $\mathbf{E}$ is the endmember matrix composed of p endmembers $\{\mathbf{e}_j\}_{j=1}^{p} \in \mathbf{R}_{+}^{d}$ and $\mathbf{A}$ contains the fractional abundances: $\{\mathbf{a}_i\}_{i=1}^{N} \in \mathbf{R}_{+}^{p}$, F is a function representing the mixing model and $\mathbf{e}$ represents the error. By defining function F, any mixing model can be derived. The goal of spectral unmixing is to solve for the abundance matrix $\mathbf{A}$ via its estimate $\hat{\mathbf{A}}$.

High correlation in the spectral data hamper the abundance estimation. Consider e.g., the Linear Spectral Mixing Model (LSMM):

$$\mathbf{Y} = \mathbf{E}\mathbf{A} + \mathbf{e} \tag{2}$$

Using a least-squares approach, the estimate for $\hat{\mathbf{A}}$ is given

by:

$$\hat{\mathbf{A}} = (\mathbf{E}^\top \mathbf{E})^{-1} \mathbf{E}^\top \mathbf{Y} \tag{3}$$

When measuring the hyperspectral dataset $\mathbf{Y}$, systematic effects caused by environmental and measurement conditions are often applied uniformly across all data points. These effects, along with intrinsic similarities between the spectra, cause a high correlation in $\mathbf{Y}$. As the abundances in $\mathbf{A}$ are usually not highly correlated. a high correlation of the mixed dataset $\mathbf{Y}$ forces the endmember matrix $\mathbf{E}$ to become highly correlated as well. As a result, the least-squares inversion in Eq. 3 becomes unstable, leading to poor abundance estimation.

2.2. Our Approach

The aim is to reduce the correlation of the dataset with the purpose of improving spectral unmixing results. We will use the mean spectral angle between all the spectra of $\mathbf{Y}$ as a measure for its orthogonality:

$$\text{mean spectral angle} = \frac{1}{N} \sum_{i=1}^{N} \sum_{j=1, j\neq i}^{N} \cos^{-1} \left(\frac{(\mathbf{y}_i)^\top \mathbf{y}_j}{\|\mathbf{y}_i\| \|\mathbf{y}_j\|} \right) \tag{4}$$

We propose a transformation that optimizes the mean spectral angle (see **Algorithm 1**). The algorithm is based on the removal of frequency components of the spectra. After applying the Fast Fourier Transform (FFT), each spectrum has d frequency components, corresponding to the number of spectral bands. Then, a number of frequency components (the same components for all spectra of $\mathbf{Y}$) is removed with the goal of maximizing the mean spectral angle of the data, after inverse Fourier Transform.

By removing these components, we aim to achieve two goals: zeroing-out common frequencies to remove unwanted correlations; excluding the frequencies entirely from consideration to remove unwanted spectral redundancies.

We have to note that the resulted transformed spectra can no longer be physically interpreted as reflectance spectra as they no longer obey the positivity nore the 0 to 1 conditions and no longer hold a physical meaning.

This problem can be framed as an optimization task, with the aim to maximize a loss function defined by the mean spectral angle between all spectra from $\mathbf{Y}$.

This optimization can be solved by different approaches such as Greedy Algorithms or Monte Carlo approaches. In this work, we chose genetic algorithms (GAs). GAs provide multiple advantages, notably their balance between exploration and exploitation, fast convergence, and the ability to explore a wide search space without getting stuck in local optima.

Our implementation starts by randomly initializing a population of binary strings of size d, where 1 indicates that the frequency component is kept in the final reconstruction and 0 indicates that it is removed (masked). To prevent the algorithm from eliminating all the components, it is required that a minimum number of frequencies is kept; it was empirically found that the $\log$ of the number of spectra in the dataset is a good choice for this minimum. We then compute the mean spectral angle (eq 4) of the dataset after reconstructing using the inverse Fast Fourier Transform (IFFT) on the frequency components selected to be kept by each binary string. This value is used to estimate the fitness of each string. The best-performing top 10% strings are kept (elitism), crossed over using uniform crossover, and mutated with a mutation rate of 10% to generate the next batch of binary strings while still retaining the best 10% strings from the previous generation. We also ensure that the minimum number of frequencies condition is still maintained. This process is repeated for a number of iterations or until no further improvement is made in the best fitness of the population. Finally, we return the best-performing string and the transformed data using that binary string.

3. EXPERIMENTS

3.1. The Data

To validate our method, a dataset of homogeneously mixed clay powders is applied, as published by [15], and available for download at [16]. The dataset consists of 330 mixtures of five clays: Kaolin, Roof clay, Red clay, Mixed clay, and Calcium hydroxide. These five clays have been mixed in such a way to uniformly cover the five-dimensional simplex, with a step size of 14.286%. In [15], these mixtures have been measured using 13 different sensors with a spectral range from 350 nm to 15385 nm. In this paper, we focus on the data measured using the ASD spectrometer with a spectral range from 350 nm to 2500 nm with a 1 nm radiometric resolution from 350 to 1000 nm and 3 nm spectral resolution from 1000 nm to 2500 nm. The endmembers (pure clay samples) are shown in Fig. 1. We will also limit ourselves to binary and ternary mixtures (5 pure clays, 6 mixtures for each of 10 possible binary mixture combinations and 15 mixtures for each of 10 possible ternary clay mixture combinations). Each ternary mixture combination forms a data manifold where each point of the manifold is a measured spectrum, and its position within the manifold reflects its relative abundances with respect to the endmembers. An example of a data manifold formed by mixing three clays, is shown in Fig. 2.

This dataset presents a significant challenge due to its low mean spectral angle of approximately 4.2 degrees for the mixtures, resulting in high spectral similarity. Such similarity complicates the direct application of traditional unmixing algorithms, making this dataset an ideal test case for our approach. Additionally, the availability of high-quality ground truth abundances allows for objective performance evaluation.

Algorithm 1 Genetic Algorithm for Frequency Selection

Input: Spectra, Population size, Generations, Mutation rate, Crossover rate, Elitism rate, Minimum frequency count (log of the number of spectra)
Output: Spectra with improved orthogonality and selected frequencies
Compute FFT of the spectra
Initialize a population of binary strings with at least the minimum number of spectral frequencies

Function *Fitness Calculation (individual)*:
Reconstruct spectra with IFFT and compute mean spectral angle as fitness score
return Fitness score

Function *Elite Selection (population)*:
Evaluate fitness and select top individuals based on elitism rate
return Selected individuals

Function *Crossover (parent1, parent2)*:
Generate offspring by combining parents, ensuring minimum frequency count
return Offspring

Function *Mutation (individual)*:
Apply mutation, ensuring minimum frequency count
return Mutated individual

Initialize best fitness as negative infinity and best individual as None
Initialize a counter for generations without improvement
for each generation **do**
    Evolve the population
    for each individual **do**
        Calculate fitness
        if fitness is better than best fitness **then**
            Update best fitness and individual, reset counter
        else
            Increment counter
        end if
    end for
    if counter exceeds threshold **then**
        break ▷ Stopping criterion
    end if
end for
Reconstruct spectra using the best individual
return Best reconstructed spectra and binary string

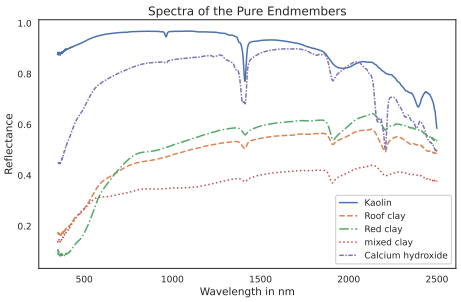

Fig. 1. Spectra of pure endmembers in the dataset.

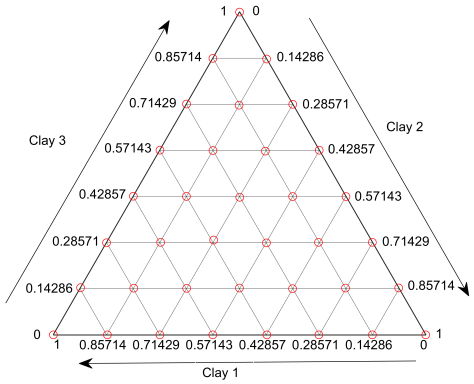

Fig. 2. Diagram of manifold constructed with mixtures of 3 clays.

3.2. Experimental Results

To visualize the effect of the proposed transform, a Principal Component Analysis (PCA) plot of a real data manifold (the one with Kaolin, Red clay and Calcium hydroxide as endmembers) and its transformation is shown in Fig. 3. One can observe that the manifold gains intrinsic structure after applying the proposed transformation, possibly improving the relation between the relative position of a data point in the manifold and its fractional abundances.

Additionally, we applied four unmixing algorithms: FCLSLU [2], Hapke model [7], MLM [3], and PPNM [5] to all the binary and ternary mixtures from the dataset. Next, the proposed transformation is applied to all spectra and the unmixing algorithms are reapplied. The applied quantitative measure is the mean Root Mean Square Error (RMSE) between the estimated abundances ($\hat{\mathbf{A}}$) obtained from both the original and transformed data, and the ground truth fractional abundances ($\mathbf{A}$):

$$\text{Abundance RMSE} = \sqrt{\frac{1}{pN}\sum_{j=1}^{p}\sum_{i=1}^{N}\left(\hat{\mathbf{A}}_{ij} - \mathbf{A}_{ij}\right)^2} \times 100 \tag{5}$$

The aggregated results are presented in Table 1.

Model	Mean RMSE (Original)	Mean RMSE (Transformed)
FCLSLU	11.7752	**9.6985**
Hapke	21.9145	**17.6136**
MLM	11.3119	**9.9233**
PPNM	9.8031	**9.4549**

Table 1. Comparison of abundance RMSE between original and transformed data for the different unmixing models (best performances are highlighted in bold).

Fig. 3. PCA plot of an original and transformed data manifold.

We also explored the robustness to noise of the proposed transformation by progressively adding noise to the data with decreasing signal-to-noise ratios (SNR) from 100 dB to 30 dB. At each SNR step, the unmixing methods are applied to the noisy and the transformed noisy data. Fig. 4 visualizes the data manifold from the same ternary mixture combination as in Fig. 3. It can be observed that the transformed manifold remained stable up to 40 dB, but began to collapse and loose its intrinsic structure at higher noise levels (35 dB and 30 dB). This is also reflected in the quantitative results, averaged over all manifolds, shown in Table 2 where the performance dropped at the 40dB noise level.

SNR	Model	Mean RMSE (Original)	Mean RMSE (Transformed)
100	FCLSLU	11.7752	**9.7731**
	Hapke	21.9145	**15.5377**
	MLM	11.312	**10.1214**
	PPNM	**9.8032**	9.8062
50	FCLSLU	11.7691	**9.1515**
	Hapke	21.9112	**19.464**
	MLM	11.3028	**10.2564**
	PPNM	9.7217	**9.2426**
40	FCLSLU	11.7452	**14.6008**
	Hapke	21.9175	**20.3883**
	MLM	**11.2685**	17.6093
	PPNM	**9.0697**	14.8643
35	FCLSLU	**11.7138**	17.2822
	Hapke	26.2287	**17.9566**
	MLM	**11.2669**	20.1509
	PPNM	**8.8815**	17.6037
30	FCLSLU	**11.6041**	20.5277
	Hapke	28.9998	**20.2089**
	MLM	**11.412**	25.2274
	PPNM	**10.328**	20.6314

Table 2. Comparison of abundance RMSE between original and transformed data for the different unmixing models at different noise levels (best performances are highlighted in bold).

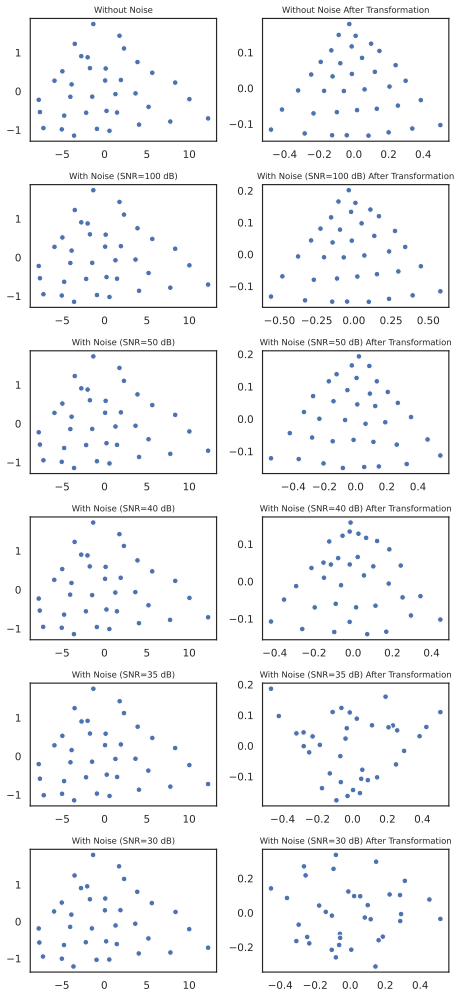

Fig. 4. Effect of noise on an original and transformed data manifold, visualized using PCA.

4. DISCUSSION

The proposed approach consistently demonstrates improved spectral unmixing results on real data in all tested mixing models, largely due to the improved orthogonality of the transformed data manifold.

Additionally, it can be observed that the transformation changes the original manifold so that the sampled points are more dispersed. This increased dispersion is the result of an increased mean spectral angle. The transform also causes the data points to be distributed more evenly. These two effects combined result in a data manifold distribution that more closely resembles the original sampling of the clay mixtures and makes it easier to establish the relationship between the position of the data in the data manifold and the abundances.

This transformation could complement the nonlinear spectral unmixing approach proposed in [17] using Bézier Surfaces, because both methods benefit from spectra that are

uniformly distributed across the data manifold. However, our method may struggle in scenarios where hyperspectral images contain abundances largely concentrated towards one or more endmembers. Additionally, while our approach performs well on clean data, its sensitivity to high noise levels (as seen in the results at 35 dB and 30 dB) is a limitation. This problem could be addressed by integrating denoising techniques to improve the signal-to-noise ratio (SNR).

5. CONCLUSIONS

In this work, we introduced a new transformation that improves the performance of unmixing algorithms by enhancing the overall orthogonality of the spectra. We validated our method on a real hyperspectral dataset and demonstrated notable improvements in performance. Future work will focus on utilizing this method to improve the performance of the nonlinear spectral unmixing approach using Bézier surfaces.

6. REFERENCES

[1] J. W. Boardman, "Geometric mixture analysis of imaging spectrometry data," in *IEEE International Geoscience and Remote Sensing Symposium*, 1994, pp. 2369–2371.

[2] D. Heinz, C.-I. Chang, and M.L.G. Althouse, "Fully constrained least-squares based linear unmixing [hyperspectral image classification]," in *IEEE 1999 International Geoscience and Remote Sensing Symposium. IGARSS'99 (Cat. No.99CH36293)*, 1999, vol. 2, pp. 1401–1403 vol.2.

[3] R. Heylen, M. Parente, and P. Gader, "A review of nonlinear hyperspectral unmixing methods," *IEEE Journal of Selected Topics in Applied Earth Observations and Remote Sensing*, vol. 7, no. 6, pp. 1844–1868, 2014.

[4] N. Dobigeon, J.Y. Tourneret, C. Richard, Jose Carlos M. Bermudez, Stephen McLaughlin, and Alfred O. Hero, "Nonlinear unmixing of hyperspectral images," *IEEE Signal Processing Magazine*, vol. 31, no. 1, pp. 82–94, JAN 2014.

[5] Y. Altmann, A. Halimi, N. Dobigeon, and J. Tourneret, "Supervised nonlinear spectral unmixing using a post-nonlinear mixing model for hyperspectral imagery," *IEEE Transactions on Image Processing*, vol. 21, no. 6, pp. 3017–3025, 2012.

[6] R. Heylen and P. Scheunders, "A multilinear mixing model for nonlinear spectral unmixing," *IEEE Transactions on Geoscience and Remote Sensing*, vol. 54, no. 1, pp. 240–251, Jan 2016.

[7] B. Hapke, "Bidirectional reflectance spectroscopy: 1. theory," *Journal of Geophysical research*, vol. 86, pp. 3039–3054, 1981.

[8] B. Rasti, B. Koirala, and P. Scheunders, "Hapkecnn: Blind nonlinear unmixing for intimate mixtures using hapke model and convolutional neural network," *IEEE Transactions on Geoscience and Remote Sensing*, vol. 60, pp. 1–15, 2022.

[9] G. M. Foody, "Relating the land-cover composition of mixed pixels to artificial neural network classification outpout," *Photogrammetric Engineering and Remote Sensing*, vol. 62, pp. 491–499, 1996.

[10] G. Licciardi and F. D. Frate, "Pixel unmixing in hyperspectral data by means of neural networks," *IEEE Transactions on Geoscience and Remote Sensing*, vol. 49, pp. 4163–4172, 2011.

[11] B. Koirala, R. Heylen, and P. Scheunders, "A neural network method for nonlinear hyperspectral unmixing," in *IEEE International Geoscience and Remote Sensing Symposium*, 2018, pp. 4233–4236.

[12] B. Koirala, M. Khodadadzadeh, C. Contreras, Z. Zahiri, R. Gloaguen, and P. Scheunders, "A supervised method for nonlinear hyperspectral unmixing," *Remote Sensing*, vol. 11, no. 20, 2019.

[13] Behnood Rasti, Bikram Koirala, Paul Scheunders, and Pedram Ghamisi, "How hyperspectral image unmixing and denoising can boost each other," *Remote Sensing*, vol. 12, no. 11, 2020.

[14] Xiang Xu, Jun Li, Changshan Wu, and Antonio Plaza, "Regional clustering-based spatial preprocessing for hyperspectral unmixing," *Remote Sensing of Environment*, vol. 204, pp. 333–346, 2018.

[15] Bikram Koirala, Behnood Rasti, Zakaria Bnoulkacem, Andréa de Lima Ribeiro, Yuleika Madriz, Erik Herrmann, Arthur Gestels, Thomas De Kerf, Sandra Lorenz, Margret Fuchs, Koen Janssens, Gunther Steenackers, Richard Gloaguen, and Paul Scheunders, "A multisensor hyperspectral benchmark dataset for unmixing of intimate mixtures," *IEEE Sensors Journal*, vol. 24, no. 4, pp. 4694–4710, 2024.

[16] "A multisensor hyperspectral benchmark dataset for unmixing of intimate mixtures," 2024, `https://github.com/VisionlabHyperspectral/Multisensor_datasets`.

[17] Bikram Koirala, Behnood Rasti, Zakaria Bnoulkacem, and Paul Scheunders, "Nonlinear spectral unmixing using bézier surfaces," *IEEE Transactions on Geoscience and Remote Sensing*, vol. 62, pp. 1–16, 2024.